Chemical Science

ROYAL SOCIETY OF CHEMISTRY

EDGE ARTICLE

View Article Online
View Journal | View Issue

Check for updates

Cite this: *Chem. Sci.*, 2022, **13**, 3589

All publication charges for this article have been paid for by the Royal Society of Chemistry

Received 5th October 2021
Accepted 24th February 2022

DOI: 10.1039/d1sc05479a

rsc.li/chemical-science

$OvoA_{Mtht}$ from *Methyloversatilis thermotolerans* ovothiol biosynthesis is a bifunction enzyme: thiol oxygenase and sulfoxide synthase activities†

Ronghai Cheng,‡[a] Andrew C. Weitz,‡[a] Jared Paris,‡[b] Yijie Tang,[b] Jingyu Zhang,[c] Heng Song,[a] Nathchar Naowarojna,[a] Kelin Li,[a] Lu Qiao,[a] Juan Lopez,[a] Mark W. Grinstaff,[a] Lixin Zhang,[c] Yisong Guo,*[b] Sean Elliott*[a] and Pinghua Liu*[a]

Mononuclear non-heme iron enzymes are a large class of enzymes catalyzing a wide-range of reactions. In this work, we report that a non-heme iron enzyme in *Methyloversatilis thermotolerans*, $OvoA_{Mtht}$, has two different activities, as a thiol oxygenase and a sulfoxide synthase. When cysteine is presented as the only substrate, $OvoA_{Mtht}$ is a thiol oxygenase. In the presence of both histidine and cysteine as substrates, $OvoA_{Mtht}$ catalyzes the oxidative coupling between histidine and cysteine (a sulfoxide synthase). Additionally, we demonstrate that both substrates and the active site iron's secondary coordination shell residues exert exquisite control over the dual activities of $OvoA_{Mtht}$ (sulfoxide synthase *vs.* thiol oxygenase activities). $OvoA_{Mtht}$ is an excellent system for future detailed mechanistic investigation on how metal ligands and secondary coordination shell residues fine-tune the iron-center electronic properties to achieve different reactivities.

Introduction

Ergothioneine and ovothiol A (**4**, **8**, Scheme 1) are naturally occurring thiol-histidine derivatives. Both of them have beneficial effects to human health. Recently, Ames proposed that ergothioneine is a longevity vitamin,[1] and exhibits protective roles in many aging associated diseases, including dementia, depression, atherosclerosis, cardiovascular disorders, and nonalcoholic fatty liver disease.[2,3] Ovothiol A inhibits cell proliferation with the concomitant activation of an autophagic process in human hepatocarcinoma cell lines, Hep-G2,[4] suggesting its potential anti-cancer activities.

Due to the growing interests in ergothioneine and ovothiol due to their biological activities,[2,3,5] the discovery of the ergothioneine and ovothiol biosynthetic pathways (Scheme 1) provides a starting point for their production through a biosynthetic approach.[6,7] Moreover, enzymes in these biosynthetic pathways are attractive from a mechanistic enzymology point of view because the C–S bond formation reactions in these two pathways are unprecedented transformations. Thus far, all attempts to trap reaction intermediates have failed because the reaction is fast and no intermediates could be observed by pre-steady state enzyme kinetics.

To address this issue, we decided to analyze and characterize enzymes from thermophilic and mesophilic organisms.[8] When enzymes from these organisms are studied at ambient temperatures, they may have slower reaction rates, allowing us to trap reaction intermediates.

In this report, we characterized a mononuclear iron enzyme from *Methyloversatilis thermotolerans* ($OvoA_{Mtht}$), an organism with an optimum growth temperature of 30–37 °C. Besides having a significantly improved thermo-stability relative to the previously reported *Erwinia tasmaniensis* $OvoA_{Eta}$,[9,10] $OvoA_{Mtht}$'s biochemical properties are also distinct from the previously reported sulfoxide synthases.[11–16] $OvoA_{Mtht}$ is a bifunctional enzyme. When cysteine is provided as the only substrate, $OvoA_{Mtht}$ catalyzes cysteine oxidation to cysteine sulfinic acid (the activity of cysteine dioxygenase, CDO). Further inclusion of histidine as the second substrate changes $OvoA_{Mtht}$ from CDO-like activity to an oxidative coupling reaction between cysteine and histidine (a sulfoxide synthase). In addition, the variation of $OvoA_{Mtht}$ activities between CDO-like and sulfoxide synthase could be modulated by either substrate/substrate analogs, or by a non-heme iron center secondary coordination shell tyrosine residue. Our subsequent biophysical characterizations using electron paramagnetic resonance (EPR) and Mössbauer spectroscopies indicate that the electronic properties of the active site iron are modulated by substrates, suggesting the change in

[a]*Department of Chemistry, Boston University, 590 Commonwealth Ave., Boston, MA 02215, USA. E-mail: pinghua@bu.edu; elliott@bu.edu*

[b]*Department of Chemistry, Carnegie Mellon University, 4400 Fifth Avenue, Pittsburgh, PA 1521, USA. E-mail: ysguo@andrew.cmu.edu*

[c]*State Key Laboratory of Bioreactor Engineering, East China University of Science and Technology, 130 Meilong Rd, Shanghai, 200237, China*

† Electronic supplementary information (ESI) available. See DOI: 10.1039/d1sc05479a

‡ These authors contributed equally to this work.

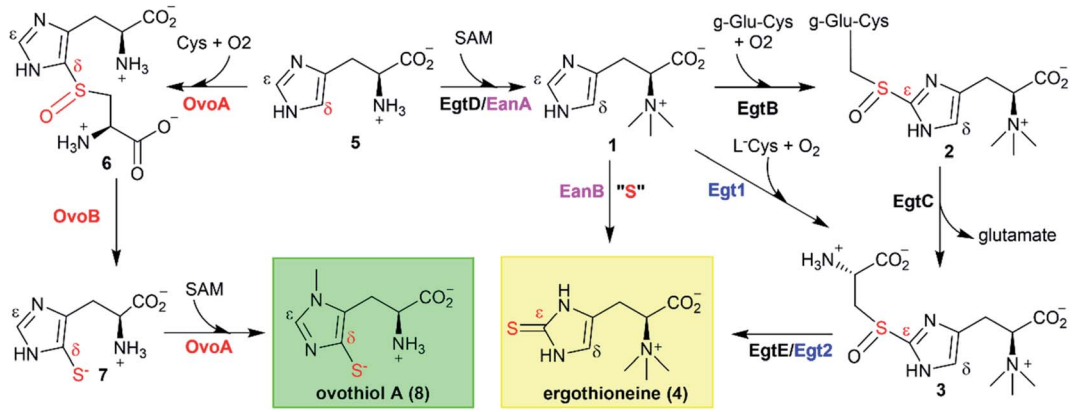

Scheme 1 Ergothioneine and ovothiol biosynthetic pathways. Two aerobic ergothioneine biosynthetic pathways: the EgtB–EgtC–EgtE-catalysis in mycobacteria, and Egt1–Egt2-catalysis in fungi; An anaerobic ergothioneine biosynthetic pathway: EanB-catalysis in sulfur bacteria; The OvoA–OvoB catalysis in the aerobic ovothiol A biosynthetic pathway.

reactivity is prompted by the substrates' close interaction with or binding to the iron center.

Results and discussion

Analysis of OvoA homologs from thermophilic/mesophilic organisms

In the last decade, one anaerobic and two aerobic[12,14,15] ergothioneine biosynthetic pathways have been discovered (Scheme 1).[5,17–19] One ovothiol biosynthetic pathway has also been biochemically characterized (Scheme 1).[9,10] In these pathways, the key step is the activation of imidazole sp^2 C–H bonds and replacing them with a C–S bond (catalyzed by EgtB,[12] Egt1,[14] EanB,[17,18] and OvoA,[9,20] Scheme 1). In the aerobic ergothioneine biosynthetic pathways from *Mycobacterium smegmatis* and *Neurospora crassa*, a non-heme iron enzyme (EgtB[12] or Egt1 (ref. 14)) catalyzes the oxidative coupling between hercynine 1 and cysteine or γ-glutamyl-cysteine to form a sulfoxide (2 or 3, Scheme 1). In the anaerobic ergothioneine biosynthetic pathway from green-sulfur bacterium *Chlorobium limicola*,[17] a rhodanese catalyzes the key C–S bond formation step using polysulfide as the direct sulfur-source (EanB-catalysis, Scheme 1, pink).[18,19] For ovothiol, thus far, only the *Erwinia tasmaniensis* ovothiol biosynthetic pathway has been biochemically characterized, with enzymes OvoA and OvoB (Scheme 1, red).[9,10,20] A mononuclear non-heme iron enzyme ($OvoA_{Eta}$) catalyzes the oxidative coupling between histidine and cysteine to sulfoxide **6** (**5** → **6**, Scheme 1).[9] Interestingly, in comparison to the ergothioneine biosynthetic enzymes (Egt1 & EgtB, Scheme 1), the $OvoA_{Eta}$ enzyme is different in both substrate selectivity and product C–S bond regioselectivity.[11,13] In addition, $OvoA_{Eta}$ is a bi-functional enzyme, catalyzing the oxidative C–S bond formation reaction (**5** → **6**, Scheme 1) and the imidazole side-chain methylation reaction (**7** → **8**, Scheme 1).[10] The second step in ovothiol biosynthesis (**6** → **7**, Scheme 1) is catalyzed by a PLP-dependent C–S lyase OvoB.

Using Egt1 (Scheme 1) from *N. crassa*,[14] OvoA (Scheme 1) from *E. tasmaniensis*,[9] and EgtB (Scheme 1) from *M. smegmatis*[12] as the query sequences, we searched for their homologs in thermophilic/mesophilic organisms. In total, we obtained 180 sequences. Using protein sequence similarity network analysis method,[21] at an *E*-value cut-off of 10^{-60}, these sequences segregate into two clusters (Fig. 1A). The larger cluster (light blue, Fig. 1A) has the biochemically characterized ergothioneine biosynthetic enzyme EgtB from *M. thermoresistibile* ($EgtB_{Mthr}$, dark blue).[22] Interestingly, $EgtB_{Cth}$,[15] an EgtB homolog from Candidatus Chloracidobacterium thermophilum (green, Fig. 1A), is located at a position bridging the major and the minor clusters, and $EgtB_{Cth}$ has been reported to have both Egt1 and EgtB activity (Scheme 1).[15] These results imply that the sequences in the small cluster (red, Fig. 1A) might be unique.

Domain structures of these five genes in the small cluster (red, Fig. 1A) were analyzed using the Pfam program (Fig. S1†).[23] They all have the DinB_2 domain and FGE-sulfatase domain, and in recently reported X-ray crystal structures of two ergothioneine sulfoxide synthases, $EgtB_{Mthr}$ and $EgtB_{Cth}$, the sulfoxide synthase active site is formed between these two domains.[15,22] Among the five genes, we focused on Refseq ID: WP_018410809.1 from *M. thermotolerans*, named as $OvoA_{Mtht}$ in this work.[24] Similar to the bifunctional $OvoA_{Eta}$ (Scheme 1), $OvoA_{Mtht}$ also has a C-terminal methyl transferase domain (Pfam family: Methyltransf_31, Fig. S1†). Moreover, in $OvoA_{Mtht}$, residues important to its sulfoxide-synthase activity are conserved, including the mono-nuclear non-heme iron ligands (His68, His159, His163) and the catalytically-relevant tyrosine (Tyr405, Fig. S2†). Structural prediction using the Phyre2 program indicated that $OvoA_{Eta}$ and $OvoA_{Mtht}$ have similar protein folding and active site environments (Fig. S3†).[25] These bioinformatic results imply that $OvoA_{Mtht}$ might be an ovothiol biosynthetic enzyme.

To provide additional support for the above prediction, using the *E. tasmaniensis* C–S lyase, $OvoB_{Eta}$, as the query sequence, we searched for OvoB homologs in the *M. thermotolerans* genome. A gene (Refseq ID: WP_026224516.1, named as $OvoB_{Mtht}$ in this work) with ~55% similarity to $OvoB_{Eta}$ was

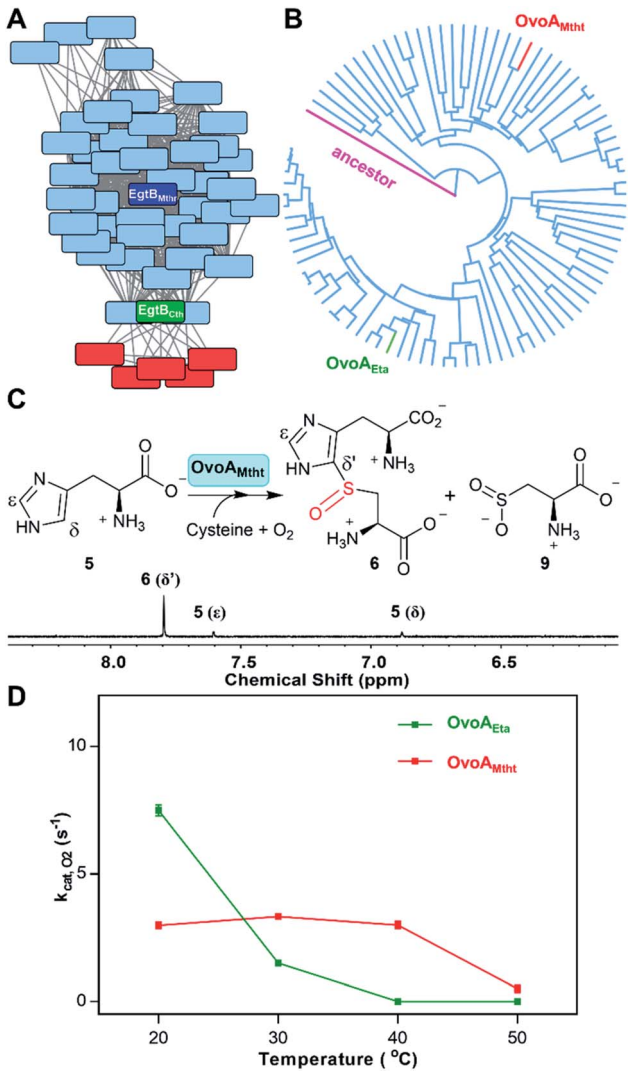

Fig. 1 Discovery of OvoA homologs through bioinformatic analysis. (A) At the *E*-value of 10^{-60}, EgtB/OvoA/Egt1 homologs from thermophilic/mesophilic strains are separated into two clusters (blue and red clusters) by protein similarity network analysis. The dark-blue box represents EgtB$_{Mthr}$, and the green box represents EgtB$_{Cth}$, which has both Egt1 and EgtB activity; (B) phylogenetic analysis in MEGA7 for OvoA$_{Mtht}$, OvoA$_{Eta}$, and their homologs;[27] (C) ^{1}H-NMR assay of OvoA$_{Mtht}$ when both cysteine and histidine are present, where OvoA$_{Mtht}$ exhibits a sulfoxide synthase activity, producing sulfoxide **6** as the major product (>90%), while at the same time, producing a small amount (<10%) of sulfinic acid **9**; the signals in ^{1}H-NMR are from the hydrogen atoms at the corresponding positions in either histidine **5** or sulfoxide **6**; (D) thermostability analysis of OvoA$_{Eta}$ and OvoA$_{Mtht}$'s sulfoxide synthase activity using histidine and cysteine as the substrates, the reaction was monitored by measuring the oxygen consumption rate. The enzyme was pre-incubated at different temperatures for 1 hour and then used for activity assays at room temperature.

identified, and it is located adjacent to the OvoA$_{Mtht}$ gene (Fig. S1B†). This bioinformatics analysis information highly suggests that these two genes in *M. thermotolerans* encode ovothiol biosynthetic enzymes.

After predicting OvoA$_{Mtht}$ and OvoB$_{Mtht}$ as the *M. thermotolerans* ovothiol biosynthetic genes, we conducted additional phylogenetic analysis of OvoA genes using the UPGMA method.[26] Sequences were randomly picked from OvoA homologs among all taxa to create the phylogenetic tree shown in Fig. 1B. OvoA$_{Mtht}$ and OvoA$_{Eta}$ genes were manually added to the sequence pool to compare the evolutionary pathway between them. Results from this analysis imply that OvoA$_{Mtht}$ is a comparatively more ancestral gene than OvoA$_{Eta}$ (Fig. 1B).

Differences between OvoA$_{Mtht}$ and the previously reported OvoA$_{Eta}$

The coding sequence of OvoA$_{Mtht}$, with codon-optimization for *E. coli* overexpression, was synthesized by Genscript and subcloned into pASK-IBA3+ vector. OvoA$_{Mtht}$ was then overexpressed and purified using a protocol similar to what we have used in OvoA$_{Eta}$ studies (Fig. S4A†).[11,13] The purified OvoA$_{Mtht}$ has 0.95 ± 0.05 equivalent of iron as determined by atomic emission spectroscopy (Fig. S4B†). After the pure OvoA$_{Mtht}$ protein was obtained, we first evaluated its predicted ovothiol sulfoxide synthase activity. Because the ovothiol sulfoxide synthase uses cysteine and histidine as the two substrates, and O_2 as the oxidant for the oxidative coupling process, OvoA$_{Mtht}$-catalysis was analyzed by three different assays: (a) ^{1}H-NMR to monitor reactions on the histidine imidazole side-chain; (b) ^{13}C-NMR assay for cysteine reactions using [β-^{13}C]-cysteine as the substrate; (c) oxygen consumption rate analysis using NeoFoxy oxygen electrode.

In an OvoA$_{Mtht}$ reaction including L-cysteine and histidine as the substrates, the ^{1}H-NMR-spectrum is indeed consistent with the predicted ovothiol sulfoxide synthase activity (Fig. 1C and S5†). In the 6–8 ppm region, the two signals are from the histidine imidazole hydrogens (~7.6 ppm and ~6.8 ppm). In the OvoA$_{Mtht}$ reaction, a new signal appears at ~7.8 ppm. Based on results reported previously on Egt1/EgtB/OvoA$_{Eta}$,[11,14] the new signal at ~7.8 ppm is from sulfoxide **6** imidazole ε-carbon C–H bond (Scheme 1), which provides the initial evidence indicating that OvoA$_{Mtht}$ is indeed the ovothiol sulfoxide synthase.

OvoA$_{Mtht}$ steady-state kinetic parameters were obtained by monitoring oxygen consumption rates using a NeoFoxy oxygen electrode. In order to rule out the oxygen consumptions caused by reductants auto-oxidation and uncoupled oxygen consumption, traces of reactions in absent of enzyme (Fig. S6A†) or cysteine substrate (Fig. S6B†) were recorded and were subtracted from the total oxygen consumption traces from enzymatic reactions. The kinetic parameters of OvoA$_{Mtht}$ using histidine and cysteine as substrates at 20 °C are: $k_{cat,O2} = 168.8 \pm 4.5$ min^{-1}; $K_{M,\ his} = 630.1 \pm 63.6$ μM and $K_{M,\ cys} = 171.6 \pm 18.6$ μM (Fig. S6†). Under our assay condition, from ^{1}H-NMR and ^{13}C-NMR analysis (Fig. S5†), >90% of the activity is sulfoxide synthase activity. Therefore, these kinetic parameters obtained from oxygen consumption assay most likely represents the kinetic parameters for OvoA$_{Mtht}$'s sulfoxide synthase activity. Because OvoA$_{Mtht}$ is from a mesophilic organism, its thermostability was also examined. The thermostabilities of OvoA$_{Mtht}$ and OvoA$_{Eta}$ protein were analyzed by nanoDSF assay and the thermal unfolding curves of OvoA$_{Mtht}$ and OvoA$_{Eta}$ indicate that the T_m of OvoA$_{Mtht}$ is ~20 °C higher than that of

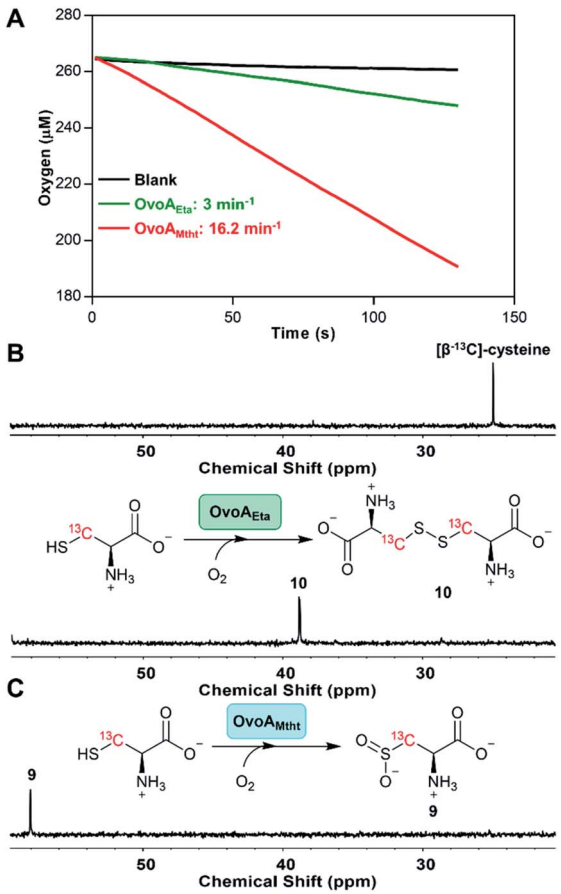

Fig. 2 Cysteine oxidation reactions by OvoA$_{Eta}$ and OvoA$_{Mtht}$ (A) oxygen consumption assay of OvoA$_{Eta}$ and OvoA$_{Mtht}$ using cysteine as the only substrate. (B) ^{13}C-NMR analysis of OvoA$_{Eta}$ reaction using [β-^{13}C]-cysteine as the substrate, which shows cystine **10** as the major product. The ^{13}C-NMR spectrum of [β-^{13}C]-cysteine (top) is included as a control. (C) ^{13}C-NMR analysis of OvoA$_{Mtht}$ reaction using [β-^{13}C]-cysteine as the substrate, which shows cysteine sulfinic acid **9** as the product.

OvoA$_{Eta}$ (Fig. S4C†). Such a difference in thermostability between OvoA$_{Mtht}$ and OvoA$_{Eta}$ were also confirmed by the oxygen consumption assay after they were pre-incubated at a certain temperature for one hour. After incubation at 30 °C for one hour, OvoA$_{Eta}$ lost most of its activity (Fig. 1D). When the temperature was further increased to 40 °C, after one hour, OvoA$_{Eta}$'s activity was completely lost. However, for OvoA$_{Mtht}$, there is barely any loss of sulfoxide synthase activity between 20–40 °C after one hour pre-incubation (the red trace, Fig. 1D).

Besides an enhanced thermostability, biochemical analysis indicated that OvoA$_{Mtht}$ is different from the previously reported OvoA$_{Eta}$ in at least two aspects.[17,25] First, when cysteine is the only substrate, OvoA$_{Eta}$ and other sulfoxide synthases (Egt1/EgtB) have a very low O_2 consumption activity (green trace, Fig. 2A),[13,14] while OvoA$_{Mtht}$ displays a very robust O_2 consumption rate when cysteine is the substrate (red trace, Fig. 2A). Second, the cysteine oxidation product from OvoA$_{Mtht}$ reaction is different from that in the OvoA$_{Eta}$ reaction (Fig. 2B *vs.* Fig. 2C). When cysteine is used as the only substrate, the OvoA$_{Eta}$ reaction product is cystine, **10**, as shown in ^{13}C-NMR spectrum from the [β-^{13}C]-cysteine reaction (OvoA$_{Eta}$ reaction in Fig. 2B). In contrast, in the OvoA$_{Mtht}$ reaction, cysteine sulfinic acid **9** is the product (Fig. 2C), which is the activity of cysteine dioxygenase enzymes (CDO). OvoA$_{Mtht}$'s CDO-like activity was further confirmed under single-turnover conditions, where OvoA$_{Mtht}$ and [β-^{13}C]-cysteine (1 : 0.9 in ratio) were mixed with an excess amount of O_2. Under this condition, cysteine sulfinic acid **9** was detected as the only product (^{13}C-NMR spectrum, Fig. S7†).

Detailed kinetic analysis of the OvoA$_{Mtht}$'s CDO-like activity gives the kinetic parameters at 20 °C of: $k_{cat,O2} = 16.2 \pm 0.2$ min^{-1} and $K_{M,\ cys} = 8.1 \pm 0.6$ mM (red trace in Fig. 2A and S8†). These kinetic parameters are at a level comparable to CDOs reported in literature.[28] In the *M. thermotolerans* genome, our analysis indicated that besides OvoA$_{Mtht}$, it does not have another copy of the CDO gene, suggesting that OvoA$_{Mtht}$ is a novel dual-function enzyme with both CDO-like and sulfoxide synthase activities.

OvoA$_{Mtht}$ characterization by EPR and Mössbauer spectroscopies

The presence of dual activities in OvoA$_{Mtht}$ (CDO-like and sulfoxide synthase activities) immediately raises the next important question: how are these two activities in OvoA$_{Mtht}$ controlled by the structural and electronic properties of the active site? As an initial step toward answering these questions, we characterized OvoA$_{Mtht}$ using Mössbauer and EPR spectroscopies.

For characterizations using Mössbauer spectroscopy, samples were prepared under anaerobic conditions by mixing ^{57}Fe-loaded OvoA$_{Mtht}$ with cysteine, histidine, or both for 5 minutes before the samples were frozen for analysis. The Mössbauer spectrum of the Fe(II)·OvoA$_{Mtht}$ complex exhibits a quadrupole doublet with a broad linewidth, suggesting some level of structural inhomogeneity at the iron-center. This broad quadruple doublet can be simulated with two species having isomer shift values (δ) of 1.22 and 1.25 mm s^{-1} and quadrupole splitting values (ΔE_Q) of 2.25 and 2.80 mm s^{-1} (species A & B, Fig. 3A and Table S1†), respectively. These Mössbauer parameters are indicative of a mononuclear high-spin ($S = 2$) ferrous iron. These parameters are also similar to those from the Fe(II)·CDO complex for cysteine dioxygenase, the Fe(II)·MDO$_{Av}$ complex for 3-mercaptopropionic acid dioxygenases (MDO), and Fe(II)·ADO reported in the literature.[29,30] The Mössbauer spectrum of the Fe(II)·OvoA$_{Mtht}$·His complex also shows a broad quadruple doublet and could be simulated by including the quadruple doublet of the Fe(II)·OvoA$_{Mtht}$ complex (~70% of the total iron) and a new doublet having $\delta = 1.24$ mm s^{-1} and $\Delta E_Q = 3.13$ mm s^{-1} (species C represented by grey trace, Fig. 3A and Table S1†). This new species is most likely due to the binding of histidine to the iron center. However, only a small fraction (~20%) of iron is converted to this His-bound state, suggesting that histidine alone does not interact with the iron-center strongly. In contrast, the Fe(II)·OvoA$_{Mtht}$·Cys complex exhibited a much sharper quadrupolar doublet. The spectral simulation suggested that ~25% of the total iron are from the Fe(II)·

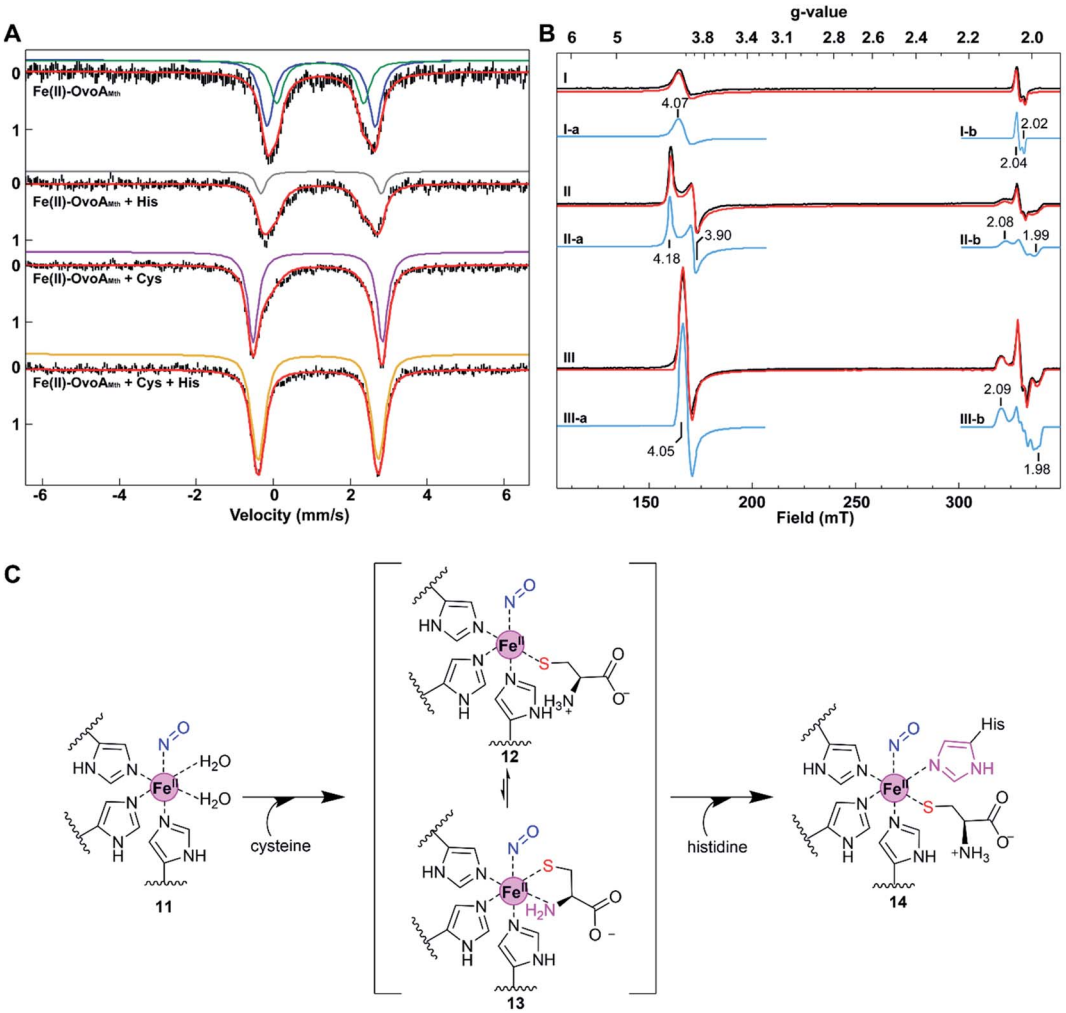

Fig. 3 The effects of substrate binding on the OvoA$_{Mtht}$ spectroscopic properties. (A) 4.2 K Mössbauer spectra of OvoA with various substrate combinations. The substrates used in these samples are labelled on the spectral traces. Samples were prepared by mixing 1 mM OvoA prepared anaerobically with 25 mM cysteine, histidine, or cysteine + histidine in 100 mM Tris buffer containing 500 mM NaCl 10% glycerol at pH 8.0. The resulting spectra have also been simulated with parameters listed in Table S1.† Black = experimental data, red: full simulation; green: species A in the Fe(II)·OvoA$_{Mtht}$ complex; blue: species B in the Fe(II)·OvoA$_{Mtht}$ complex, grey: species C for the putative Fe(II)·OvoA$_{Mtht}$·His complex; pink: species D for the putative Fe(II)·OvoA$_{Mtht}$·Cys complex; and orange: species E for the putative Fe(II)·OvoA$_{Mtht}$·Cys·His complex with Mössbauer parameters listed in Table S1.† (B) 15 K EPR spectra of NO-treated OvoA$_{Mtht}$. Trace I: enzyme only; trace II: enzyme with 0.2 mM cysteine; trace III: enzyme with 0.5 mM cysteine and 0.5 mM histidine. Black: experimental spectra; red: full simulations of experimental spectra; blue: component simulations of separate high spin (HS) and low spin (LS) iron nitrosyl species: (I/II/III-a) HS {FeNO}^{7} species. The minor $g = 2$ resonance of this species is omitted for clarity. See ESI† for full details. (I-b) Dinitrosyl iron complex impurity. (II/III-c) LS {FeNO}^{7} species associated with the presence of either Cys or Cys + His, respectively. (C) Schematic presentation of potential ligand environment changes under various conditions used in Mössbauer and EPR spectroscopic characterization.

OvoA$_{Mtht}$ complex, while the rest of the iron (~75%) exhibited a different quadruple doublet with $\delta = 1.16$ mm s^{-1} and $\Delta E_Q = 3.36$ mm s^{-1} (species D represented by the pink trace, Fig. 3A and Table S1†). The parameters of this additional doublet (species D, Fig. 3A) are in fact, similar to those of Cys-bound Fe(II) in CDO and in MDO$_{Av}$, and thus could be similarly assigned as the Fe(II)·OvoA$_{Mtht}$·Cys complex.[30,31] In the presence of both cysteine and histidine, the Mössbauer spectrum converted to a sharp quadrupolar doublet, which can be simulated with a single species having $\delta = 1.17$ mm s^{-1} and $\Delta E_Q = 3.12$ mm s^{-1}, suggesting a high structural homogeneity at the iron center in the Fe(II)·OvoA$_{Mtht}$·Cys·His complex (species E as represented by the orange trace, Fig. 3A and Table S1†).

Results from these Mössbauer characterization suggest that Cys could bind to the iron center tightly, which is a prerequisite for the CDO-like reactivity. Histidine alone may not interact with the iron strongly, as shown by the presence of species C as only a minor species. However, Cys binding facilitates His binding, which may be the key for the change of OvoA$_{Mtht}$ from CDO-like to sulfoxide synthase by promoting the C–S coupling reactivity (Fig. 2 and S5†).

To provide further evidence on how the substrate modulates the electronic properties of the iron active site, we also

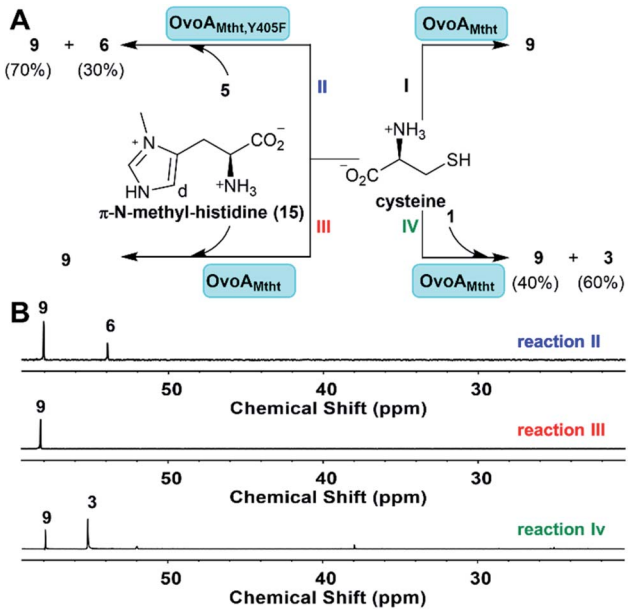

Fig. 4 Examining factors controlling OvoA$_{Mtht}$'s CDO-like and sulfoxide synthase activities. (A) Four reactions examined in this work; (B) ^{13}C-NMR analysis of OvoA$_{Mtht}$ reactions. Reaction II: OvoA$_{Mtht,Y405F}$ mutant reaction using cysteine and histidine as substrates; reaction III has π-*N*-methyl-histidine and cysteine as the substrates; and reaction IV has hercynine **1** and cysteine as the substrates.

characterized OvoA$_{Mtht}$ using EPR spectroscopy. Because Fe^{2+} is EPR silent, nitric oxide (NO) is often used as a tool in EPR characterization of mononuclear non-heme iron enzymes, where the NO-bound complex becomes EPR-active, with the additional structural benefit of NO acting as an O_2 mimic.[32,33] The Fe(II)·OvoA$_{Mtht}$ EPR spectra were collected after treating various enzyme–substrate combinations with NO from proli-NONOate, including Fe(II)·OvoA$_{Mtht}$ only, Fe(II)·OvoA$_{Mtht}$ + Cys, or Fe(II)·OvoA$_{Mtht}$ + Cys + His samples.

The Fe(II)·OvoA$_{Mtht}$ + NO sample produced an EPR spectrum with two species (trace I, Fig. 3B). The broad axial signal at $g = 4.07$ (species I-a) is typical of a $S = 3/2$ {FeNO}^{7} species (with E/D $= 0.008$, $\sigma_{E/D} = 0.005$), where the electronic configuration of the iron nitrosyl species is described using the commonly-used Enemark/Feltham notation.[34] The broad line shape can be attributed to the heterogeneity of active site, due to the lack of the bound substrate to better define the active site coordination.[35] This heterogeneity is mirrored in the Mössbauer data of the Fe(II)·OvoA$_{Mtht}$ complex in Fig. 3A. The low yield of this species (33 μM of 100 μM total enzyme) may be a function of poor NO binding in the absence of substrate, as observed in other oxygenases.[32,36] The species near $g = 2$ (species I-b, 1.4 μM) is assigned as a non-enzymatic dinitrosyl iron species (DNIC).[37,38] Its presence is common in NO adducts of Fe-containing enzymes and is a minor impurity in the OvoA$_{Mtht}$ samples.[39]

Relative to the spectrum of the Fe(II)·OvoA$_{Mtht}$ + NO sample, the resultant Fe(II)·OvoA$_{Mtht}$·Cys + NO sample's EPR spectrum (trace II) showed a clear change in the $g = 4$ region, as demonstrated by a more rhombic (E/D $= 0.021$, $\sigma_{E/D} = 0.003$) $S = 3/2$ species, having signals at $g = 4.18$, 3.90 (species II-a, Fig. 3B). This new EPR signal was generated in near full-yield (100 μM, Table S2†), which suggests that Cys binding facilitate O_2/NO binding and this result is consistent with the presence of CDO-like activity in OvoA$_{Mtht}$. Additionally, a new low

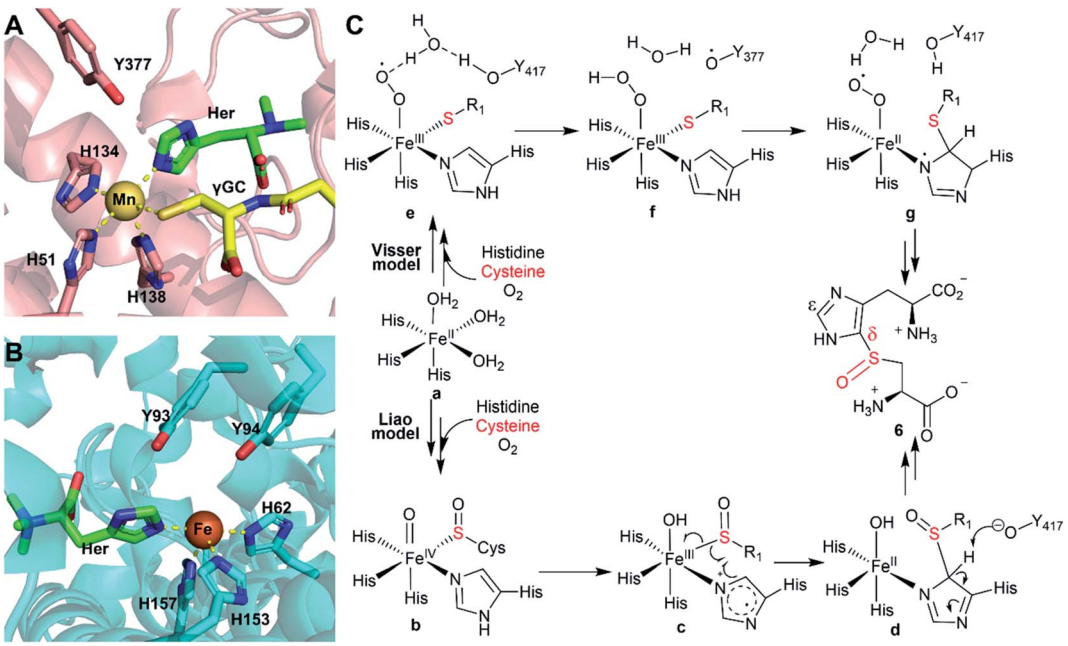

Scheme 2 (A) Crystal structure of EgtB$_{Mthr}$ with hercynine (Her) and gamma-gluatmyl-cysteine (γGC) binding to the active site (PDB ID: 4X8D).[22] (B) Crystal structure of EgtB$_{Cth}$ with hercynine binding to the active site (PDB ID: 6O6M).[15] (C) Proposed mechanism for OvoA$_{Eta}$-catalysis based on information from structural information of EgtB$_{Mthr}$ and EgtB$_{Cth}$ and related computational studies.

spin feature near $g = 2$ (species II-b) is present in the Fe(II)·$OvoA_{Mtht}$·Cys + NO sample as a minority species (7 μM, Table S2†). The g values of this feature (2.08, 2.03, 1.99) are reminiscent of those for the $S = 1/2$ $\{FeNO\}^7$ species commonly associated CDO enzymes having bidentate-bound cysteine (Fig. S9A and Table S3†).[30,32,40] There is a strong literature precedence that correlates low spin $\{FeNO\}^7$ to bidentate (S/N) bound Cys (*via* thiolate S and amino N). Consequently, our EPR data suggest that the majority of Cys bound to $OvoA_{Mtht}$ is most likely monodentate. Recently, with MDO, the yield of the low spin form was affected by the protonation state of tyrosine residues in the active site.[30] Similar interactions with nearby amino acid residues may explain the presence of this species in $OvoA_{Mtht}$. For these reasons, when cysteine binds in $OvoA_{Mtht}$, we propose the Fe(II)·$OvoA_{Mtht}$·Cys adduct is a mixture of mono-dentate and bidendate complexes. In the reported crystal structures of ergothioneine sulfoxide synthases, the non-heme iron centers are coordinated by three protein histidine residues,[15,22,28,32,41,42] which are also conserved in $OvoA_{Mtht}$. Based on this information, we propose the geometric model for the Fe(II)·$OvoA_{Mtht}$-·Cys complex as shown in Fig. 3C, in which Cys binds to the iron-center as a mixture of mono-dendate and bi-dendate complexes.

When more than two equivalents of cysteine were added, the yield of the $S = 3/2$ species decreased while the yield of a $S = 1/2$ species near $g = 2.04$ increased (Fig. S10†). We attribute this additional species at $g \sim 2$ to a DNIC species based on literature precedence,[43–46] where the excess Cys may be binding adventitiously to the Fe, along with NO. To support this interpretation, we have independently formed this species by mixing free Fe, cysteine, and NO under anaerobic conditions (Fig. S11†). Therefore, the DNIC species with $g = 2$ region (Fig. S10†) is most likely irrelevant to $OvoA_{Mtht}$-catalysis.

Interestingly, upon introducing NO to the Fe(II)·$OvoA_{Mtht}$-·Cys·His complex, both the $g \sim 4$ and $g \sim 2$ signals (trace III, Fig. 3B) change significantly from that observed in the Fe(II)·$OvoA_{Mtht}$·Cys + NO sample. The rhombic signal at $g \sim 4$ in Fe(II)·$OvoA_{Mtht}$·Cys + NO sample (species II-a) changes to a sharper axial signal at $g = 4.05$ following the addition of histidine (species III-a). In addition, the Fe(II)·$OvoA_{Mtht}$·Cys·His + NO sample has a new $S = 1/2$ species (species III-b,19 μM, in Table S4†), having g-values 2.096, 2.029, 1.985 (Fig. 3B and S9B†). Samples of 0.05, 0.1, and 0.5 mM His in the presence of 0.5 mM Cys show that both species grow in a concentration-dependent manner (Fig. S12 and Table S4†).

Upon introduction of histidine into the Fe(II)·$OvoA_{Mtht}$·Cys complex, spectroscopic changes in both the high spin and low spin $\{FeNO\}^7$ EPR signals are consistent with having both histidine and cysteine as iron-ligands as proposed in Fig. 3C. An OvoA crystal structure has yet to be reported, however crystal structures of two sulfoxide synthases in ergothioneine biosynthesis ($EgtB_{Mthr}$[22] & $EgtB_{Cth}$[15]) are available. In the EgtB crystal structures, the mononuclear non-heme iron-center is coordinated by three protein histidine residues. Sequence alignments between $EgtB_{Mthr}$, $EgtB_{cth}$ and $OvoA_{Mtht}$ indicated that the three iron histidine ligands are conserved in these three proteins (Fig. S2†). The EPR spectra of the Fe(II)·$OvoA_{Mtht}$·Cys + NO sample suggests the cysteine is predominantly bound in the HS/monodentate binding mode. Such a configuration would then allow for the additional histidine to bind at the active site as well. The remaining vacant site is presumably for O_2 binding and activation (as evidenced by NO binding to the active site in the EPR samples). Together, the spectroscopic information obtained in our Mössbauer and EPR characterization of $OvoA_{Mtht}$ support the second step of our $OvoA_{Mtht}$-schematic model in Fig. 3C, in which both cysteine and histidine bind to the iron-center as mono-dentate ligands.

Modulate $OvoA_{Mtht}$ reaction by substrate analogs and Fe-secondary coordination shell residues

$OvoA_{Mtht}$ is a bifunctional enzyme with both CDO-like and sulfoxide synthase activities (Fig. 1C *vs.* Fig. 2C), which is very different from previously reported ergothioneine and ovothiol sulfoxide synthases (EgtB/Egt1/$OvoA_{Eta}$).[47,48] Most of these sulfoxide synthases (EgtB/Egt1/$OvoA_{Eta}$) do not have CDO-like activity when cysteine is provided as the only substrate, while they do oxidize cysteine slowly to produce cystine as the oxidation product. In $EgtB_{Mthr}$, a very low level of sulfur oxidation activity (~1% of $OvoA_{Mtht}$'s CDO-like activity) was reported.[22,49] In EgtB/Egt1/$OvoA_{Eta}$, upon mutating the active site tyrosine to a phenylalanine residue, the resulting mutants show ~100% CDO-like activity.[47,49] Therefore, in EgtB/Egt1/$OvoA_{Eta}$, the sulfoxide synthase and CDO-like activities are primarily modulated by an iron-center's secondary coordination shell residue, a tyrosine residue.

In the absence of a $OvoA_{Mtht}$ crystal structure, we created a homology model using the Phyre2 program (Fig. S3†).[25] According to this model, Tyr405 in $OvoA_{Mtht}$ is the corresponding active site tyrosine. The $OvoA_{Mtht,Y405F}$ mutant was overexpressed and purified using a protocol similar to that used in wild type $OvoA_{Mtht}$. $OvoA_{Mtht}$ activities were then examined under four different conditions (Fig. 4A):

(I) $OvoA_{Mtht}$ using cysteine as the only substrate;

(II) $OvoA_{Mtht,Y405F}$ mutant using cysteine and histidine as co-substrates;

(III) $OvoA_{Mtht}$ using cysteine and π-*N*-methyl-histidine as co-substrates;

(IV) $OvoA_{Mtht}$ using cysteine and hercynine as co-substrates.

For the $OvoA_{Mtht,Y405F}$ mutant, when histidine and cysteine are co-substrates, the kinetic parameters from the O_2 consumption assay are: $k_{cat,O2}$ of 162.6 ± 2.1 min^{-1}; $K_{M,\ his}$ = 152.4 ± 11.0 μM and $K_{M,\ cys}$ = 290.0 ± 16.1 μM. These $OvoA_{Mtht,Y405F}$ mutant kinetic parameters (Fig. S13†) are similar to those of the wild type $OvoA_{Mtht}$ (Fig. 1C). However, different from all previously reported EgtB/Egt1 or OvoA enzymes,[13,47–49] whose active site tyrosine mutants show ~100% CDO-like activity, the $OvoA_{Mtht,Y405F}$ mutant exhibits sulfoxide synthase/CDO-like product formation in a ratio of 3 : 7 (reaction II, Fig. 4).

From the spectroscopic characterization (Fig. 3), it is clear that the iron-center's electronic properties are modulated by both substrates. To provide further evidence supporting the above conclusion, we also examined $OvoA_{Mtht}$ activities using

two histidine analogs, π-*N*-methyl-histidine **15**, and trimethylhistidine (hercynine, **1**). π-*N*-Methyl-histidine was synthesized according to the literature procedure (Fig. S14†).[50] The reaction (reaction III, Fig. 4) was monitored by ^{1}H-NMR, ^{13}C-NMR, and the O_2 consumption rate assay. The ^{1}H-NMR spectrum indicates that when π-*N*-methyl-histidine and cysteine are co-substrates, $OvoA_{Mtht}$ exhibits no sulfoxide synthase activity (Fig. S15†). However, the oxygen consumption rate of this reaction (reaction III, Fig. 4) is almost the same as the $OvoA_{Mtht}$ native reaction (Fig. 1C), with kinetic parameters for reaction III in Fig. 4 of: $k_{cat,O2} = 99.2 \pm 2.7$ min^{-1}; K_M, π-*N*-methyl-histidine $= 112.2 \pm 17.4$ μM and K_M, cys $= 249.1 \pm 28.3$ μM (Fig. S16†). ^{13}C-NMR indicated that the only product in this reaction is cysteine sulfinic acid **9**. Therefore, in $OvoA_{Mtht}$, when π-*N*-methyl-histidine is used to replace histidine, $OvoA_{Mtht}$ also changes from a sulfoxide synthase to a CDO. Intriguingly, π-*N*-methyl-histidine stimulates the $OvoA_{Mtht}$'s CDO-like activity by nearly 200-fold ($k_{cat,O2}/K_M$ for cysteine) relative to the cysteine-only reaction (reaction I, Fig. 4). As a matter of fact, under this condition, $OvoA_{Mtht}$'s CDO-like activity is 1–2 order of magnitude greater than other CDOs reported in literature.[28] The difference between these reactions (Fig. 1C *vs.* reaction I & III in Fig. 4) indicate the histidine or its analogs modulate the $OvoA_{Mtht}$ activities between CDO-like and sulfoxide synthase. Moreover, binding of histidine/histidine analogs also increases the O_2 consumption rate by 1–2 orders of magnitude.

Different from π-*N*-methyl-histidine **15**, whose methylation is on the side-chain, hercynine **1** is methylated at its α-amino group. Because the imidazole ring of histidine is likely an iron ligand, π-*N*-methyl-histidine **15** might modulate the electronic properties of the iron-center. Hercynine's methylation is on its α-amino group and any effects observed for hercynine reaction should be the secondary coordination shell effects (*e.g.*, hydrogen bonding, hydrophobicity, or ionic interactions between the substrate α-amino group and its nearby residues). When hercynine and cysteine are used as the substrate, $OvoA_{Mtht}$ exhibits a sulfoxide synthase/CDO-like ratio of 4 : 6 (reaction IV, Fig. 4). Interestingly, ^{1}H-NMR analysis clearly indicated that $OvoA_{Mtht}$'s sulfoxide synthase regioselectivity changes from the imidazole δ-position in the native reaction (Fig. 1C) to ε-position in Fig. 4 reaction IV (Fig. S17†). The kinetic parameters from the O_2 consumption assay are: $k_{cat,O2} = 47.8 \pm 4.2$ min^{-1}; $K_{M,\ hercynine} = 185.9 \pm 17.2$ μM and $K_{M,\ cys} = 1060.2 \pm 121.2$ μM (Fig. S18†).

Conclusion

In this work, based on bioinformatics analysis of 180 potential sulfoxide synthases from thermophilic/mesophilic organisms,[21] we selected $OvoA_{Mtht}$ from *M. thermotolerans* for biochemical and spectroscopic characterization. $OvoA_{Mtht}$ is biochemically distinct from the previously reported sulfoxide synthases (EgtB/Egt1/$OvoA_{Eta}$) in several aspects. First, for EgtB/Egt1/$OvoA_{Eta}$ reported in previous studies, when cysteine is provided as the only substrate, the O_2 consumption rate is very slow, and the oxidation product is cystine **10**.[13,47–49] However, when cysteine is the only substrate provided, the O_2 consumption rate in the $OvoA_{Mtht}$-catalysis is at least 1–2 orders of magnitude faster than that of EgtB/Egt1/$OvoA_{Eta}$ enzymes. Moreover, under this condition, cysteine sulfinic acid **9** instead of cystine **10** is the $OvoA_{Mtht}$ reaction product. In the *M. thermotolerans* genome, our analysis does not identify an additional CDO gene, which suggests that $OvoA_{Mtht}$ may satisfy the CDO requirements of *M. thermotolerans*. The kinetic parameters of $OvoA_{Mtht}$'s CDO-like activity are comparable to those CDOs in the literature examples.[28] The high cysteine K_M for $OvoA_{Mtht}$ is also consistent with the role of CDO as a detoxification enzyme to remove excess cysteine when its concentration reaches a high level.

The second unique feature of $OvoA_{Mtht}$ is that upon further introduction of histidine to the Fe(II)·$OvoA_{Mtht}$·Cys complex, $OvoA_{Mtht}$ switches from a CDO-like to a sulfoxide synthase. As demonstrated by Mössbauer and EPR spectroscopies, the iron-center electronic properties are modulated by both substrates (Fig. 3). It has been reported that in EgtB/Egt1/$OvoA_{Eta}$, their CDO-like and sulfoxide synthase activities are controlled by a secondary coordination shell residue to the mononuclear non-heme iron center (Tyr377 in $EgtB_{Mthr}$ and Tyr93 and Tyr94 in $EgtB_{Cth}$, Scheme 2).[15,48,49] With the previously reported systems, mutation of the active site tyrosine residue(s) to phenylalanine, the sulfoxide synthase activity is abolished, and the mutant exhibits almost exclusively the CDO-like activity. In contrast, the $OvoA_{Mtht,Y405F}$ still has sulfoxide synthase activity, displaying a sulfoxide synthase/CDO-like activity in a ratio of 3 : 7. Interestingly, upon replacing histidine by π-*N*-methyl-histidine to the Fe(II)·$OvoA_{Mtht}$·Cys complex, π-*N*-methyl-histidine changes $OvoA_{Mtht}$ from sulfoxide synthase back to 100% CDO-like again. Moreover, π-*N*-methyl-histidine binding increases $EgtB_{Mthr}$'s CDO-like reactivity by ~200-fold than the case where cysteine is the only substrate (reaction III *vs.* reaction I, Fig. 4). Therefore, in $OvoA_{Mtht}$, the activities between sulfoxide synthase and CDO-like are modulated by iron-center ligands and secondary coordination shell tyrosine residue(s), while the iron-ligands seem to play a more dominant role in $OvoA_{Mtht}$ in controlling the partition between sulfoxide synthase and CDO-like activities.

In recent years, a few mechanistic models have been proposed for ergothioneine and ovothiol sulfoxide synthases, with two representative models (Scheme 2) being suggested by Visser *et al.*[51] and Liao *et al.*,[52] respectively. The Visser model suggests that thioether formation is the first half of this reaction.[51] In contrast, the Liao model[52] proposes that sulfenic acid formation initiates the reaction. Both models involve the active site tyrosine for catalysis, while doing so with distinct functions. In the Visser model, the active site tyrosine plays a redox role and an inverse deuterium isotopic effect was predicted for ^{2}H labelled histidine. The Liao model involves the active site tyrosine in acid/base catalysis and a primary ^{2}H-labeled isotope effect as high as 5.7 was predicted for ^{2}H-labeled histidine.[52] With tyrosine analogs incorporated using the amber-suppressor method, we previously examined this relationship in $OvoA_{Eta}$-catalysis. Our observation of an inverse deuterium isotope effect is more consistent with the Visser model in $OvoA_{Eta}$-catalysis.[48,51] However, in Ovo_{Mtht}, we have found new experimental results where sulfoxide synthase activity is maintained in the Tyr → Phe mutant. As this active site Tyr is invoked in both

mechanistic models, our results suggest there may be other interactions that guide product formation. In this paper, we have presented two new avenues to be explored further: (1) modulation of the Fe electronic properties (using π-*N*-methylhistidine) and (2) noncovalent interactions between the substrate molecule and nearby amino acid residues (using hercynine).

Both Liao[52] and Liu[53] groups cautioned that the reaction pathway might be very sensitive to the detailed active site structure and the active site dynamics. Because $OvoA_{Mtht}$'s sulfoxide synthase and CDO-like activities could be modulated by both iron-ligands and its secondary coordination shell residues, it offers an excellent system for future structure–function relationship studies to provide experimental evidence for refinement of these mechanistic models (Scheme 2).

Experimental

Detailed experimental procedures are included in the ESI.†

Data availability

Data supporting this article have been uploaded as part of the ESI.†

Author contributions

R. C., N. N., K. L., L. Q., and J. L., conducted biochemical studies. R. C., A. C. W., J. P., and Y. T. conducted spectroscopic studies. J. Z. and H. S. synthesized substrates and substrate analogues. R. C. A. C. W., M. W. G., Y. G., S. J. E., and P. L. wrote the manuscript with feedback from all other authors.

Conflicts of interest

There are no conflicts to declare.

Acknowledgements

This work is partially supported by the National Science Foundation (CHE-2004109 to P. Liu, CHE-1654060 to Y. Guo) and National Institute of Health (R35-GM136294 to S. Elliott, and GM140040 to P. Liu).

Notes and references

1 B. N. Ames, *Proc. Natl. Acad. Sci. U. S. A.*, 2018, **115**, 10836–10844.
2 I. K. Cheah and B. Halliwell, *Biochim. Biophys. Acta*, 2012, **1822**, 784–793.
3 I. K. Cheah and B. Halliwell, *Antioxidants*, 2020, **9**(595).
4 G. L. Russo, M. Russo, I. Castellano, A. Napolitano and A. Palumbo, *Mar. Drugs*, 2014, **12**, 4069–4085.
5 N. Naowarojna, R. Cheng, L. Chen, M. Quill, M. Xu, C. Zhao and P. Liu, *Biochemistry*, 2018, **57**, 3309–3325.
6 I. Castellano and F. P. Seebeck, *Nat. Prod. Rep.*, 2018, **35**, 1241–1250.
7 N. Tanaka, Y. Kawano, Y. Satoh, T. Dairi and I. Ohtsu, *Sci. Rep.*, 2019, **9**, 1–10.
8 Y. Gumulya, J. M. Baek, S. J. Wun, R. E. S. Thomson, K. L. Harris, D. J. B. Hunter, J. B. Y. H. Behrendorff, J. Kulig, S. Zheng, X. M. Wu, B. Wu, J. E. Stok, J. J. De Voss, G. Schenk, U. Jurva, S. Andersson, E. M. Isin, M. Boden, L. Guddat and E. M. J. Gillam, *Nat. Catal.*, 2018, **1**, 878–888.
9 A. Braunshausen and F. P. Seebeck, *J. Am. Chem. Soc.*, 2011, **133**, 1757–1759.
10 N. Naowarojna, P. Huang, Y. Cai, H. Song, L. Wu, R. Cheng, Y. Li, S. Wang, H. Lyu, L. Zhang, J. Zhou and P. Liu, *Org. Lett.*, 2018, **20**, 5427–5430.
11 H. Song, M. Leninger, N. Lee and P. Liu, *Org. Lett.*, 2013, **15**, 4854–4857.
12 F. P. Seebeck, *J. Am. Chem. Soc.*, 2010, **132**, 6632–6633.
13 H. Song, A. S. Her, F. Raso, Z. Zhen, Y. Huo and P. Liu, *Org. Lett.*, 2014, **16**, 2122–2125.
14 W. Hu, H. Song, A. Sae Her, D. W. Bak, N. Naowarojna, S. J. Elliott, L. Qin, X. Chen and P. Liu, *Org. Lett.*, 2014, **16**, 5382–5385.
15 N. Naowarojna, S. Irani, W. Hu, R. Cheng, L. Zhang, X. Li, J. Chen, Y. J. Zhang and P. Liu, *ACS Catal.*, 2019, **9**, 6955–6961.
16 A. R. Stampfli, K. V. Goncharenko, M. Meury, B. N. Dubey, T. Schirmer and F. P. Seebeck, *J. Am. Chem. Soc.*, 2019, **141**, 5275–5285.
17 R. Burn, L. Misson, M. Meury and F. P. Seebeck, *Angew. Chem., Int. Ed.*, 2017, **56**, 12508–12511.
18 R. Cheng, L. Wu, R. Lai, C. Peng, N. Naowarojna, W. Hu, X. Li, S. A. Whelan, N. Lee, J. Lopez, C. Zhao, Y. Yong, J. Xue, X. Jiang, M. W. Grinstaff, Z. Deng, J. Chen, Q. Cui, J. Zhou and P. Liu, *ACS Catal.*, 2020, 8981–8994, DOI: 10.1021/acscatal.0c01809.
19 R. H. Cheng, R. Lai, C. Peng, J. Lopez, Z. H. Li, N. Naowarojna, K. L. Li, C. Wong, N. Lee, S. A. Whelan, L. Qiao, M. W. Grinstaff, J. Y. Wang, Q. Cui and P. H. Liu, *ACS Catal.*, 2021, **11**, 3319–3334.
20 G. T. M. Mashabela and F. P. Seebeck, *Chem. Commun.*, 2013, **49**, 7714–7716.
21 H. J. Atkinson, J. H. Morris, T. E. Ferrin and P. C. Babbitt, *PLoS One*, 2009, **4**, e4345.
22 K. V. Goncharenko, A. Vit, W. Blankenfeldt and F. P. Seebeck, *Angew. Chem., Int. Ed.*, 2015, **54**, 2821–2824.
23 J. Mistry, S. Chuguransky, L. Williams, M. Qureshi, G. A. Salazar, E. L. L. Sonnhammer, S. C. E. Tosatto, L. Paladin, S. Raj, L. J. Richardson, R. D. Finn and A. Bateman, *Nucleic Acids Res.*, 2020, **49**, D412–D419.
24 N. V. Doronina, E. N. Kaparullina and Y. A. Trotsenko, *Int. J. Syst. Evol. Microbiol.*, 2014, **64**, 158–164.
25 L. A. Kelley, S. Mezulis, C. M. Yates, M. N. Wass and M. J. E. Sternberg, *Nat. Protoc.*, 2015, **10**, 845–858.
26 P. H. Sneath and R. R. Sokal, *Numerical taxonomy. The principles and practice of numerical classification*, 1973.
27 S. Kumar, G. Stecher and K. Tamura, *Mol. Biol. Evol.*, 2016, **33**, 1870–1874.
28 C. A. Joseph and M. J. Maroney, *Chem. Commun.*, 2007, 3338–3349.

29 Y. F. Wang, I. Davis, Y. Chan, S. G. Naik, W. P. Griffith and A. M. Liu, *J. Biol. Chem.*, 2020, **295**, 11789–11802.
30 S. Sardar, A. Weitz, M. P. Hendrich and B. S. Pierce, *Biochemistry*, 2019, **58**, 5135–5150.
31 E. P. Tchesnokov, A. S. Faponle, C. G. Davies, M. G. Quesne, R. Turner, M. Fellner, R. J. Souness, S. M. Wilbanks, S. P. de Visser and G. N. L. Jameson, *Chem. Commun.*, 2016, **52**, 8814–8817.
32 B. S. Pierce, J. D. Gardner, L. J. Bailey, T. C. Brunold and B. G. Fox, *Biochemistry*, 2007, **46**, 8569–8578.
33 D. Arciero, A. Orville and J. Lipscomb, *J. Biol. Chem.*, 1985, **260**, 14035–14044.
34 J. Enemark and R. Feltham, *Coord. Chem. Rev.*, 1974, **13**, 339–406.
35 M. D. Krzyaniak, B. E. Eser, H. R. Ellis, P. F. Fitzpatrick and J. McCracken, *Biochemistry*, 2013, **52**, 8430–8441.
36 M. Costas, M. P. Mehn, M. P. Jensen and L. Que, *Chem. Rev.*, 2004, **104**, 939–986.
37 D. R. Truzzi, N. M. Medeiros, O. Augusto and P. C. Ford, *Inorg. Chem.*, 2021, **60**, 15835–15845.
38 C. E. Tinberg, Z. J. Tonzetich, H. Wang, L. H. Do, Y. Yoda, S. P. Cramer and S. J. Lippard, *J. Am. Chem. Soc.*, 2010, **132**, 18168–18176.
39 B. S. Pierce, B. P. Subedi, S. Sardar and J. K. Crowell, *Biochemistry*, 2015, **54**, 7477–7490.
40 E. J. Blaesi, J. D. Gardner, B. G. Fox and T. C. Brunold, *Biochemistry*, 2013, **52**, 6040–6051.
41 C. R. Simmons, Q. Liu, Q. Huang, Q. Hao, T. P. Begley, P. A. Karplus and M. H. Stipanuk, *J. Biol. Chem.*, 2006, **281**, 18723–18733.
42 S. Ye, X. Wu, L. Wei, D. M. Tang, P. Sun, M. Bartlam and Z. H. Rao, *J. Biol. Chem.*, 2007, **282**, 3391–3402.
43 T. R. Bryar and D. R. Eaton, *Can. J. Chem.*, 1992, **70**, 1917–1926.
44 A. R. Butler and I. L. Megson, *Chem. Rev.*, 2002, **102**, 1155–1166.
45 S. Lu, E. Libby, L. Saleh, G. Xing, J. M. Bollinger and P. Moënne-Loccoz, *J. Biol. Inorg Chem.*, 2004, **9**, 818–827.
46 N. Reginato, C. T. McCrory, D. Pervitsky and L. Li, *J. Am. Chem. Soc.*, 1999, **121**, 10217–10218.
47 L. Chen, N. Naowarojna, H. Song, S. Wang, J. Y. Wang, Z. X. Deng, C. M. Zhao and P. H. Liu, *J. Am. Chem. Soc.*, 2018, **140**, 4604–4612.
48 L. Chen, N. Naowarojna, B. Chen, M. Xu, M. Quill, J. Wang, Z. Deng, C. Zhao and P. Liu, *ACS Catal.*, 2019, **9**, 253–258.
49 K. V. Goncharenko and F. P. Seebeck, *Chem. Commun.*, 2016, **52**, 1945–1948.
50 H. C. Beyerman, A. Vanzon and L. Maat, *Recl. Trav. Chim. Pays-Bas*, 1972, **91**, 246–250.
51 A. S. Faponle, F. P. Seebeck and S. P. de Visser, *J. Am. Chem. Soc.*, 2017, **139**, 9259–9270.
52 W. J. Wei, P. E. M. Siegbahn and R. Z. Liao, *Inorg. Chem.*, 2017, **56**, 3589–3599.
53 G. Tian, H. Su and Y. Liu, *ACS Catal.*, 2018, **8**, 5875–5889.